

# Analytic Model of the Universal Structure of Turbulent Boundary Layers

Victor S. L'vov, Itamar Procaccia and Oleksii Rudenko  
*The Department of Chemical Physics, The Weizmann Institute of Science, Rehovot 76100, Israel*

Turbulent boundary layers exhibit a universal structure which nevertheless is rather complex, being composed of a viscous sub-layer, a buffer zone, and a turbulent log-law region. In this letter we present a simple analytic model of turbulent boundary layers which culminates in explicit formulae for the profiles of the mean velocity, the kinetic energy and the Reynolds stress as a function of the distance from the wall. The resulting profiles are in close quantitative agreement with measurements over the entire structure of the boundary layer, without any need of re-fitting in the different zones.

**Introduction:** Theoretical physicists tend to consider turbulence in the context of the idealized model of isotropic and homogenous fluid flows at large Reynolds numbers. In part this is due to the apparent existence of universal, anomalous scaling exponents which characterize correlation and structure functions in fully developed turbulent flows. It is also easier to disregard the effects of walls which introduce essential anisotropies and inhomogeneities. Needless to say, all realistic turbulent flows are neither homogeneous nor isotropic. A problem of extreme interest for both technological applications and from the point of view of basic science is “wall-bounded” turbulence, with the theoretical model of a flat infinite wall playing a key role. This problem presents also fascinating universal features, see Fig.1, but traditionally it was more popular in the engineering rather than in the physics community. There are fascinating open problems in wall-bounded turbulence. The present Letter attempts at finding a simple model that affords an analytic calculation of the universal profiles of the mean velocity, the turbulent energy and the Reynolds stress as a function of the distance from the wall.

The theory that we construct begins with the equations of fluid mechanics and focuses on the momentum and energy fluxes using the conservation laws for these quantities as a guidance for developing an appropriate model. In gross substance this approach is not new, and indeed a number of ingredients are borrowed from the literature. The model that we end up with is however improved compared to previous results in the sense that it provides analytic predictions for the above-mentioned profiles in the entire boundary layer, without re-fitting in the different zones. It should be stressed at this point that one cannot expect a universal model to apply for all turbulent boundary values problem. For instance, the understanding of drag reduction by additives calls for a slightly modified model that stresses the effects of the additives. The present contribution offers what we consider a simplest model that is constructed to best describe Newtonian wall-bounded turbulence with enough richness to capture all the essential universal profiles of the quantities of interest. One advantage of the model that will be demonstrated in future publications is that it can be naturally generalized to describe stratified turbu-

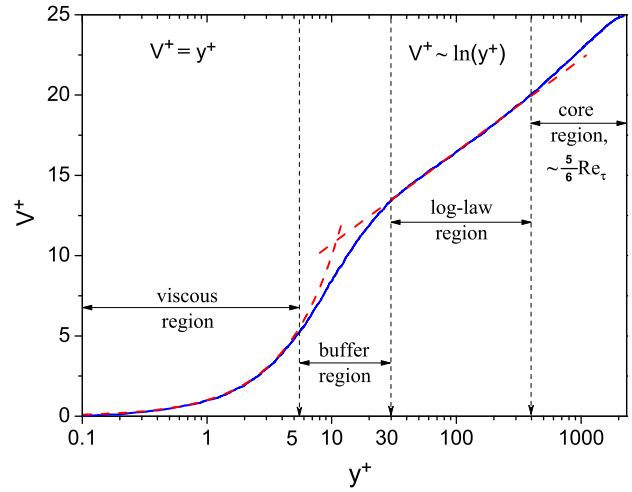


FIG. 1: A sketch of the characteristic regions appearing in a turbulent boundary layer. The continuous line represents the mean velocity profile  $V^+(y^+)$  [in the wall units, Eq. (4)] taken from direct numerical simulation at  $Re_\tau = 2320$ , [1]. The “viscous region” ends when the linear law  $V^+ = y^+$  begins to deviate from the continuous line at  $y^+ \approx 6$ . The “log-law region” ends approximately at  $1/6$  of the channel height, i.e.  $y^+ \approx Re_\tau/6$ . At this point and deeper towards the channel centerline the dimensionless momentum flux to the wall,  $\mathcal{P}^+ = 1 - y^+/Re_\tau$  (see Eq. (24)), deviates appreciable from unity.

lent boundary layers caused by, say, temperature gradients, heavy particles, etc, with applications to interesting problems like sand storms in deserts, snow fall in a windy days or water flow in a heavily silt-laden rivers.

**Equations and definitions:** The starting point are the Navier-Stokes equations for an incompressible fluid velocity  $\mathbf{U}(\mathbf{r}, t)$ ,

$$\frac{\partial \mathbf{U}}{\partial t} + (\mathbf{U} \cdot \nabla) \mathbf{U} = -\frac{\nabla p}{\rho} + \nu \Delta \mathbf{U}, \quad \nabla \cdot \mathbf{U} = 0, \quad (1)$$

where  $\rho$  is the fluid density,  $p = p(\mathbf{r}, t)$  – the pressure and  $\nu$  is the kinematic viscosity. We follow the standard strategy of Reynolds considering the velocity as a sum of its average (over time) and a fluctuating part:

$$\mathbf{U}(\mathbf{r}, t) = \mathbf{V}(\mathbf{r}) + \mathbf{u}(\mathbf{r}, t), \quad \mathbf{V}(\mathbf{r}) \equiv \langle \mathbf{U}(\mathbf{r}, t) \rangle. \quad (2)$$

We also introduce the conventional *viscous scale*  $\ell_\tau$  and *friction velocity*  $u_\tau$

$$u_\tau \equiv \sqrt{P(0)/\rho}, \quad \ell_\tau \equiv \nu/u_\tau, \quad (3)$$

where  $P(0)$  is the wall shear stress – the flux of the mechanical momentum at the wall. This quantity depends on the type of turbulent boundary layer (pressure driven or driven by the upper boundary, etc). The velocity and the distance from the wall are then measured in *wall units*

$$\mathbf{U}^+ \equiv \mathbf{U}/u_\tau, \quad y^+ \equiv y/\ell_\tau, \quad p^+ \equiv p/(\rho u_\tau^2), \quad \nabla^+ \equiv \ell_\tau \nabla. \quad (4)$$

In wall units the Navier-Stokes equation is now dimensionless, and the stationary version takes the form

$$(\mathbf{U}^+ \cdot \nabla^+) \mathbf{U}^+ = -\nabla^+ p^+ + \Delta^+ \mathbf{U}^+. \quad (5)$$

The averaged equation for the mean velocity looks like

$$(\mathbf{V}^+ \cdot \nabla^+) \mathbf{V}^+ = \Delta^+ \mathbf{V}^+ - \langle \mathbf{u}^+ \cdot \nabla^+ \mathbf{u}^+ \rangle - \nabla^+ \langle p^+ \rangle. \quad (6)$$

Besides the mean velocity one needs to consider correlation functions. It turns out that important features of wall bounded turbulence, like the mean velocity profile, thermal conductivity, turbulent transport of matter, etc., are determined by velocity fluctuations on relatively large scales, and the statistics of the latter do not deviate too much from Gaussian statistics. Thus an economic description of these features can be reached on a level of second order correlation functions. Therefore, in addition to the mean velocity profile, we will be interested in the detailed description of two additional quantities, the turbulent energy and the Reynolds stress tensor:

$$K^+ \equiv \langle |\mathbf{u}^+|^2 \rangle / 2, \quad W_{ij}^+ \equiv \langle u_i^+ u_j^+ \rangle. \quad (7)$$

**Balance equations for the Reynolds stress:** Subtracting Eq. (6) from Eq. (5), multiplying by a fluctuating velocity component  $u_j^+$  and averaging, results in the equation satisfied by the Reynolds stress:

$$(\mathbf{V}^+ \cdot \nabla^+) W_{ij}^+ = P_{ij}^+ + \mathcal{R}_{ij}^+ - \varepsilon_{ij}^+ + \partial_k T_{ijk}^+, \quad (8)$$

where the tensors of the energy production,  $P_{ij}^+$ , of the pressure-rate-of-strain,  $\mathcal{R}_{ij}^+$  and of the Reynolds-stress dissipation  $\varepsilon_{ij}^+$ , are

$$\begin{aligned} P_{ij}^+ &\equiv -W_{ik}^+ \partial_k V_j^+ + W_{jk}^+ \partial_k V_i^+, \\ \mathcal{R}_{ij}^+ &\equiv \langle \tilde{p}^+ (\partial_j u_i^+ + \partial_i u_j^+) \rangle, \quad \varepsilon_{ij}^+ \equiv 2 \langle \partial_k u_i^+ \partial_k u_j^+ \rangle, \end{aligned} \quad (9)$$

and  $\tilde{p} \equiv p - \langle p \rangle$  denotes the pressure fluctuations. The last term  $T_{ijk}^+$  presents spatial energy fluxes. We will neglect it throughout the turbulent boundary layer; it is indeed small in the log-layer, but comparable to other terms in the buffer and viscous sub-layers. The model will be constructed such as to compensate for this neglect in those regions where the term is significant. The bonus

of neglecting this term is enormous since this keeps the theory *local*, without partial derivatives.

The modeling of the various terms appearing in Eq. (8) has attracted considerable attention over the years, and we only briefly summarize how this is done. The Poisson's equation for the fluctuating pressure follows from the equation of the fluctuating part of the velocity field,  $\mathbf{u}$ , which is obtained by subtracting Eq. (6) from (5):

$$\Delta^+ \tilde{p}^+ = -\nabla_i^+ \nabla_j^+ (u_i^+ u_j^+ - \langle u_i^+ u_j^+ \rangle) + V_i^+ u_j^+ + V_j^+ u_i^+. \quad (10a)$$

The homogeneous solution of this equation is responsible for sound, a phenomenon of very little consequence for turbulent dynamics at low Mach numbers. The inhomogeneous solution includes two parts,  $\tilde{p}^+ = \tilde{p}_{uu}^+ + \tilde{p}_u^+$ :

$$\tilde{p}_{uu}^+ \propto u_i^+ u_j^+ - \langle u_i^+ u_j^+ \rangle, \quad \tilde{p}_u^+ \propto V_i^+ u_j^+ + V_j^+ u_i^+. \quad (10b)$$

Correspondingly the pressure-rate-of-strain tensor (9) consist of two terms:

$$\mathcal{R}_{ij}^+ = R_{ij}^{\text{RI}+} + R_{ij}^{\text{IP}+}. \quad (11a)$$

The first of these is known as the “Return-to-Isotropy” tensor,  $R_{ij}^{\text{RI}+}$ , that depends on the triple-velocity correlator  $\langle u_i u_j u_k \rangle$ . Its evaluation in terms of the objects of the theory calls for a closure, and following time-honored tradition [2] we adopt for it the simple Rota form

$$R_{ii}^{\text{RI}+} \simeq -\gamma_{\text{RI}} (3 W_{ii}^+ - W^+), \quad W^+ \equiv \text{Tr}\{W_{ij}^+\}, \quad (11b)$$

in which  $\gamma_{\text{RI}}$  is some characteristic nonlinear frequency that will be specified later. The tensor  $R_{ij}^{\text{RI}+}$  is traceless and therefore the frequency  $\gamma_{\text{RI}}$  must be the same for all diagonal components of  $R_{ii}^{\text{RI}+}$ . There is no reason however to assume that off-diagonal terms have the same frequency. Therefore, following [3], we assert that

$$R_{ij}^{\text{RI}+} \simeq -3 \tilde{\gamma}_{\text{RI}} W_{ij}, \quad i \neq j, \quad (11c)$$

with, generally speaking,  $\tilde{\gamma}_{\text{RI}} \neq \gamma_{\text{RI}}$ .

The traceless “Isotropization-of-Production” tensor,  $R_{ij}^{\text{IP}+}$  has a structure that is very similar to the production tensor  $\mathcal{P}_{ij}^+$ , Eq. (9), and thus traditionally it is modeled in terms of  $\mathcal{P}_{ij}^+$  [2]:

$$R_{ij}^{\text{IP}+} \simeq -C_{\text{IP}} (3 \mathcal{P}_{ij}^+ - \mathcal{P}^+ \delta_{ij}), \quad \mathcal{P}^+ \equiv \text{Tr}\{\mathcal{P}_{ij}^+\}. \quad (11d)$$

The dissipation tensor  $\varepsilon_{ij}^+$  is estimated differently far from the wall and near it. Far from the wall and for large Reynolds numbers the turbulent flow can be considered approximately isotropic. Therefore, the tensor  $\varepsilon_{ij}^+$  should be approximately diagonal,

$$\varepsilon_{ij}^+ = \gamma^+ W^+ \delta_{ij}. \quad (12a)$$

Under stationary conditions the rate of turbulent kinetic energy dissipation is equal to the energy input at the

outer scale, estimated as  $\langle u_i u_j u_k \rangle / \ell$  where the outer scale of turbulence  $\ell$  is estimated as the distance to the wall  $y$ . Therefore, the natural estimate of  $\gamma^+$  involves the triple-velocity correlator,

$$\gamma^+ \sim \frac{\langle uuu \rangle^+}{y \langle uu \rangle^+} \Rightarrow \gamma^+ = b \frac{\sqrt{W^+}}{y^+}. \quad (12b)$$

Similarly, we can estimate the Return-to-Isotropy frequencies  $\gamma_{\text{RI}}^+$  and  $\tilde{\gamma}_{\text{RI}}^+$  in Eqs. (11b) and (11c). Having in mind that the precise structure (tensorial contraction, etc.) of the equation for  $\gamma^+$  is different from that of the equations for  $\gamma_{\text{RI}}^+$  and  $\tilde{\gamma}_{\text{RI}}^+$ , we should involve different numerical prefactors:

$$\gamma_{\text{RI}}^+ = b_{\text{RI}} \sqrt{W^+} / y^+, \quad \tilde{\gamma}_{\text{RI}}^+ = \tilde{b}_{\text{RI}} \sqrt{W^+} / y^+. \quad (13)$$

Close to the wall, in the viscous sub-layer  $y^+ \leq 30$ , the estimates change due to the direct viscous contribution of the largest eddies at that distance, which is of the order of the distance  $y^+$  itself. For these eddies we can estimate  $\nabla^2$  operator as  $(\tilde{a}/y)^2$ , where  $\tilde{a}$  is a new fitting constant. For simplicity we account for this contribution only in off-diagonal terms, which do not include the nonlinear part (see Eq. (12a)). In this way we will have:

$$\varepsilon_{ij}^+ = \tilde{\Gamma}^+ W_{ij}^+, \quad i \neq j, \quad (14a)$$

with  $\tilde{\Gamma}^+ = (\tilde{a}/y)^2$ . Here we have to recall that we neglected the spatial energy transfer term, which played an important role in the viscous sublayer, essentially compensating viscous damping. In order to account for this effect on a qualitative level we suppress the direct viscous damping by a factor  $W/W_*$  (here  $W_*$  is the asymptotical value of  $W$  in the lag-low region) in some power  $\zeta$ :

$$\Gamma^+ = (\tilde{a}/y^+)^2 \sqrt{W^+ / W_*^+}. \quad (14b)$$

Our choice  $\zeta = \frac{1}{2}$  is dictated by the simplicity of the analytical treatment of resulting algebraical model. Posteriorly, our idea of implicit accounting for the energy flux (with  $\zeta = \frac{1}{2}$ ) in Eq. (14b) is supported by a good agreement of the model prediction for the energy profile in the viscous and buffer layers with the DNS data without additional fitting parameters, see the insert on Fig. 3.

**Plane geometry and the balance of momentum:** For plane geometry the mean velocity is oriented in the (stream-wise)  $\hat{\mathbf{x}}$  direction and depends only on the vertical (wall-normal) coordinate  $y$ :  $\mathbf{V} = V(y) \hat{\mathbf{x}}$ . For such flows all the averages are functions of  $y^+$  only. An interesting special example is a channel flow of height  $2L$  and infinite extent in the span-wise direction. Due to the symmetry in the span-wise direction  $z \rightarrow -z$ ,  $W_{xz}^+ = W_{zz}^+ = 0$ . From Eq. (6) for  $V$  (integrated over  $y^+$ )

one gets the exact balance equation for the mechanical-momentum

$$P^+(y^+) = S^+ - W_{xy}^+, \quad \text{where} \quad (15)$$

$$S^+(y) \equiv \frac{dV^+}{dy^+}, \quad P^+(y^+) \equiv 1 - \frac{y^+}{\text{Re}_\tau}, \quad \text{Re}_\tau \equiv \frac{L u_\tau}{\nu}.$$

The flat geometry also simplifies the production term defined in Eq. (9):

$$\mathcal{P}_{ij}^+ = -S^+ (W_{iy}^+ \delta_{jx} + W_{jy}^+ \delta_{ix}). \quad (16)$$

**Final set of equations:** Substituting everything into Eq. (8) we get the following set of model equations:

$$3\gamma_{\text{RI}}^+ W_{xx}^+ = (\gamma_{\text{RI}}^+ - \gamma^+) W^+ - 2(1 - 2C_{\text{IP}}) S^+ W_{xy}^+, \quad (17a)$$

$$3\gamma_{\text{RI}}^+ W_{yy}^+ = (\gamma_{\text{RI}}^+ - \gamma^+) W^+ - 2C_{\text{IP}} S^+ W_{xy}^+, \quad (17b)$$

$$3\gamma_{\text{RI}}^+ W_{zz}^+ = (\gamma_{\text{RI}}^+ - \gamma^+) W^+ - 2C_{\text{IP}} S^+ W_{xy}^+, \quad (17c)$$

$$0 = (\tilde{\Gamma}^+ + 3\tilde{\gamma}_{\text{RI}}^+) W_{xy}^+ + (1 - 3C_{\text{IP}}) S^+ W_{yy}^+. \quad (17d)$$

Summing up Eqs. (17a), (17b) and (17c) [or, equivalently, taking the trace of Eq. (8)] one gets

$$3\gamma^+ W^+ = -2S^+ W_{xy}^+. \quad (18)$$

#### Choice of the log-law parameters $b$ , $b_{\text{RI}}$ and $\tilde{b}_{\text{RI}}$ :

At this point we can fit three  $b$ -parameters responsible for the solution in the asymptotical log-law region  $30 < y^+ < \text{Re}_\tau/6$  for sufficiently large Reynolds numbers. In this region  $\tilde{\Gamma}^+$  can be neglected, and solution of Eqs. (17) takes the form

$$W_{xx}^+ = \frac{(1 - 2C_{\text{IP}})b + b_{\text{RI}}}{b + 3b_{\text{RI}}} W_*^+, \quad (19a)$$

$$W_{yy}^+ = W_{zz}^+ = \frac{C_{\text{IP}}b + b_{\text{RI}}}{b + 3b_{\text{RI}}} W_*^+, \quad (19b)$$

$$W_{xy}^+ = -b\kappa (W_*^+)^{3/2} = -1, \quad (19c)$$

$$S_*^+ = \frac{1}{\kappa y^+}, \quad \text{where} \quad (19d)$$

$$\kappa = \sqrt{\frac{2(1 - 3C_{\text{IP}})(C_{\text{IP}}b + b_{\text{RI}})}{3W_*^+ b \tilde{b}_{\text{RI}} (b + 3b_{\text{RI}})}}. \quad (19e)$$

To determine  $b$ -parameters, we used the following data:

1. The numerical values of  $W_*^+ = 6.85$  and von-Karman constant  $\kappa = 0.436$  can be taken from the direct numerical simulations (DNS) reported in [4];

2. The detailed analysis of experimental, DNS and large-eddy-simulation data, made in Ref. [3], yields the conclusion that with a good accuracy one can take

$$W_{xx}^+ = 2W_{yy}^+ = 2W_{zz}^+ = W_*^+/2; \quad (20)$$

3. The suggested in the literature (see, e.g. [2]) value of  $C_{\text{IP}}$  is  $\frac{1}{5}$ . Our analysis showed that all profiles are very

insensitive to a particular choice of  $C_{\text{IP}}$  around value 0.2. Therefore for simplicity we take

$$C_{\text{IP}} = 1/5. \quad (21\text{a})$$

All this knowledge enables us to find  $b$ ,  $b_{\text{RI}}$  and  $\tilde{b}_{\text{RI}}$ :

$$b = \frac{2}{3 \kappa W_*^{3/2}} \approx 0.085, \quad (21\text{b})$$

$$b_{\text{RI}} = 4(1 - 3C_{\text{IP}})b \approx 0.136, \quad (21\text{c})$$

$$\tilde{b}_{\text{RI}} = \frac{(1 - 3C_{\text{IP}})\sqrt{W_*^+}}{12\kappa} \approx 0.200. \quad (21\text{d})$$

For future purpose we introduce a parameter

$$\tilde{b} \equiv \frac{\tilde{b}_{\text{RI}}}{1 - 3C_{\text{IP}}} = \frac{\sqrt{W_*^+}}{12\kappa} = 0.500. \quad (21\text{e})$$

**General solution:** With chosen parameters (21) the formal solution of the system (15), (17) in the entire turbulent boundary layer is:

$$W^+ = 2W_{xx}^+ = 4W_{yy}^+ = 4W_{zz}^+, \quad (22\text{a})$$

$$W_{xy}^+ = -\frac{3\gamma^+ W^+}{2S^+}, \quad S^{+2} = 15\gamma^+ \left( \tilde{\Gamma}^+ + 3\tilde{\gamma}_{\text{RI}}^+ \right). \quad (22\text{b})$$

The last equation comes from the solvability condition for the system of Eqs. (17):  $\text{Det} = 0$ . Introduce:

$$v^+ \equiv \sqrt{W^+}, \quad v_*^+ \equiv \sqrt{W_*^+}, \quad r \equiv 1 + \frac{\tilde{a}^2}{3\tilde{b}_{\text{RI}} v_*^+ y^+}. \quad (23)$$

Then

$$W_{xy}^+ = -\frac{W^+}{2} \sqrt{\frac{b}{2\tilde{b}r}}, \quad S^+ = \frac{3v^+}{y^+} \sqrt{2\tilde{b}r}, \quad (24)$$

and Eq. (15) transforms into:

$$v^{+2} + 12\tilde{b}r v^+ / y^+ - P^+ \sqrt{8\tilde{b}r/b} = 0. \quad (25)$$

This is just a quadratic equation for  $v^+ = \sqrt{W^+}$  with a unique positive solution:

$$v^+ = \sqrt{P^+ \sqrt{\frac{8\tilde{b}}{b} r} + \left( \frac{6\tilde{b}}{y^+} r \right)^2} - \frac{6\tilde{b}}{y^+} r. \quad (26)$$

### Comparison of the model and simulations:

Clearly, a model with only 4 (or 5 if  $C_{\text{IP}}$  is counted in) fit parameters cannot fit perfectly the profiles of all the physical quantities that can be measured. Therefore the actual value of the only remained parameter  $\tilde{a}$  should be determined with a choice of the characteristics of turbulent boundary layers that we desire to describe best. Foremost in any modeling should be the mean velocity profile  $V^+$  which is of crucial importance in a wide variety of transport phenomena. Therefore we chose the

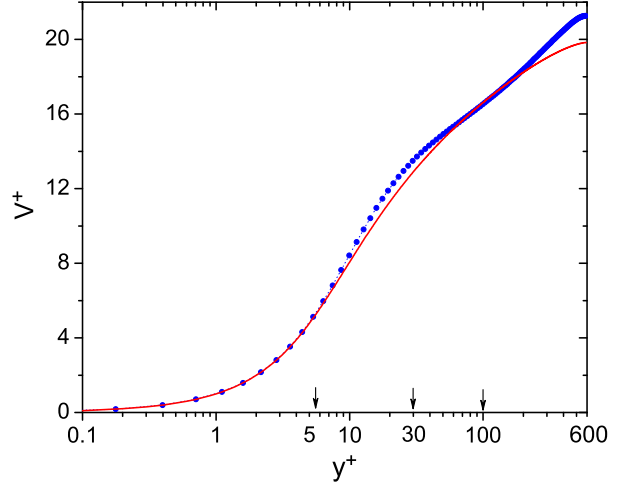


FIG. 2: Mean velocity profiles  $V^+(y^+)$ : The dotted line reproduces the results of direct numerical simulations [4] for  $\text{Re}_\tau = 590$ , the solid line is the analytical prediction of the model with  $\tilde{a} = 7.4$  and the values (21) of  $b$ ,  $b_{\text{RI}}$  and  $\tilde{b}_{\text{RI}}$ .

value of  $\tilde{a}$ , from the best fit of  $V^+(y^+)$  in the (quasi) straight logarithmic region  $30 < y^+ < 100$ :

$$\tilde{a} = 7.4. \quad (27)$$

Resulting mean velocity profile  $V^+(y^+) = \int_0^{y^+} S^+(\xi) d\xi$ , in which  $S^+(\xi)$  is given by (24), is shown in Fig. 2 by solid line for  $\text{Re}_\tau = 590$ . The dotted line represents data taken from direct numerical simulations [4], for the same  $\text{Re}_\tau = 590$ . There is no significant difference between these plots in the viscous sublayer, buffer and outer layers, where  $y^+ \lesssim 300$  i.e. in about 50% of the channel half-width  $L^+ = \text{Re}_\tau = 590$ . This robustness of the mean velocity profile  $V^+(y^+)$  is a consequence of the fact that  $V^+(y^+)$  is an integral of the mean shear  $S^+$  which is described very well both in the viscous and the outer layers.

Notice that our model does not describe the upward deviation from the log-low which is observed near the mid-channel (of about 5-6 units in  $V^+$ ). We consider this minor disagreement as an acceptable price for the simplicity of the model which neglects the spatial energy transport term toward the centerline of the channel. This transport is the only reason for some turbulent activity near the centerline where both the Reynolds stress  $W_{xy}$  and  $S$  vanish due to symmetry. Just at the center line the source term in our energy equation,  $-2SW_{xy}$ , is zero, and the missing energy transport term is felt.

The plots in Fig. 2 have a reasonably straight logarithmic region from  $y^+ \approx 30$  to  $y^+ \approx 100$ . On the other hand, the Reynolds stress profile at the same  $\text{Re}_\tau = 590$  shown in Fig. 3, has no flat region at all. Such a flat region is expected in the true asymptotic regime of  $\text{Re}_\tau \rightarrow \infty$ , where  $W^+ = -1$ . Therefore if one plots the

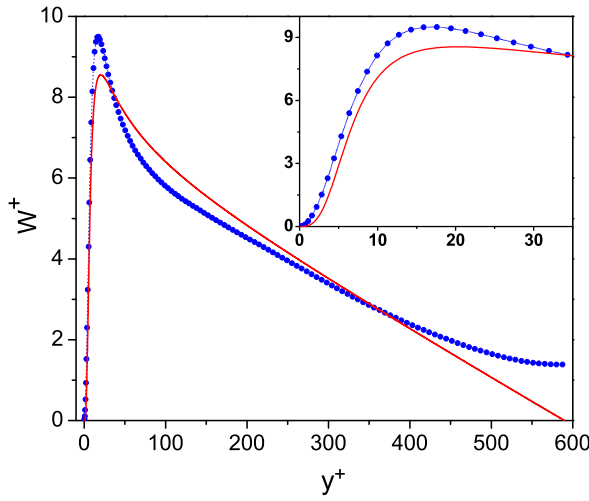


FIG. 3: The trace of the Reynolds-stress tensor (twice the total kinetic energy density): The dotted blue line reproduces the results of direct numerical simulations [4] at  $Re_\tau = 590$ , the solid red line is analytical prediction with  $\tilde{a} = 7.4$ . The insert shows the buffer layer behavior in more detail. Notice, that there is no plateau in these plots, meaning that these values of  $Re_\tau$  are not large enough to have a true scale-invariant log-law region.

model profiles  $V^+$  at different  $Re_\tau$  and fits them by log-linear profiles

$$V^+(y^+) = \kappa^{-1} \ln(y^+) + B, \quad (28)$$

one can get a  $Re_\tau$ -dependence of the “effective” intercept  $B \Rightarrow B(Re_\tau)$  in the von-Kármán log-law (28). We think that this explains why measured value of the intercept depends on the Reynolds number and on the flow geometry (channel vs. pipe): both in direct numerical simulations and in physical experiments one usually does not reach high enough values of  $Re_\tau$ .

At this point  $\tilde{a}$  and all three  $b$ -parameters are already chosen from the information about mean velocity profile and  $y^+$ -independent values of the Reynolds stress tensor in the log-law region in the limit  $Re_\tau \rightarrow \infty$ . Our results for the kinetic energy profile  $W^+$ , and the Reynolds stress profile, shown in Figs. 3 and 4 by red solid lines, in the entire TBL for finite  $Re_\tau$  value (590) is the prediction of our model without any additional fit parameters. On the same Figs. the DNS results [4] are shown by blue dotted lines. Having this in mind we consider the achieved agreement in the entire TBL as an encouraging indication that the proposed model really accounts for the important basic physics of the problem.

**Summary:** In summary we presented an analytic model of the physics of wall-bounded turbulence in a Newtonian fluid, based entirely on the balance of energy and momentum fluxes with the production and the dissipation. The model has one blatant simplification which

is the neglect of the spatial energy fluxes. The gain is

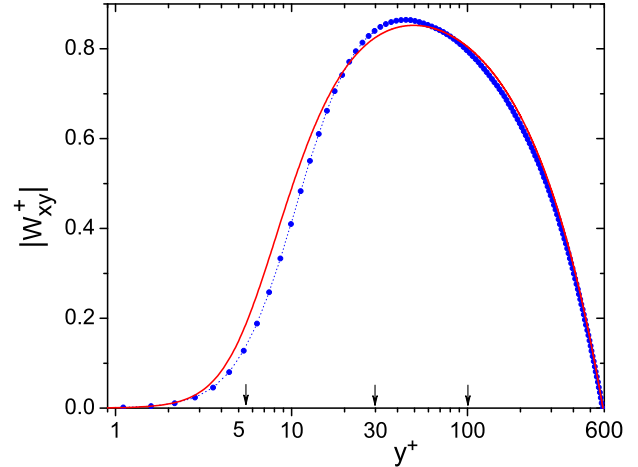


FIG. 4: The Reynolds stress  $|W_{xy}^+|$ : The dotted blue line represents results from direct numerical simulations [4] for  $Re_\tau = 590$ , the solid red line represents the prediction of the analytical model with  $\tilde{a} = 7.4$ . There is no pronounced log-law region where a plateau  $|W_{xy}^+| = 1$  is expected. Instead  $|W_{xy}^+|$  reaches only the value 0.85 around  $y^+ \approx 50$ . This means that in this region the viscous transport is still essential, but the total momentum flux is still below its (dimensionless) maximum value:  $\max(\mathcal{P}^+) = 1$ .

enormous – we get a local model that can be solved analytically to find the profiles of the mean velocity, the turbulent fluctuations and the Reynolds stress as a function of the distance from the wall, with all the boundary layer represented without re-fitting in the various regions. The reason of the success of this simple model is that we have learned how to compensate the neglect of the spatial flux in the buffer and the viscous region by an increase in the dissipative terms. In future work we will demonstrate the utility of this simple model in a variety of important wall-bounded flows.

**Acknowledgements:** This research is supported by the US-Israel Binational Science Foundation.

---

- [1] K. Iwamoto, N. Kasagi, and Y. Suzuki, Direct numerical simulation of turbulent channel flow  $Re_\tau = 2320$ , *Proc. 6th Symp. Smart Control of Turbulence* Tokyo, March 6-9, 2005, pp. 327-333.
- [2] S.B. Pope, *Turbulent Flows*, 1st ed. (Cambridge University Press, 2000).
- [3] V.S. L'vov, A. Pomyalov, I. Procaccia and S.S. Zilitinkevich, *Phys. Rev. E*, **73**, 016303 (2006).
- [4] R.G. Moser, J. Kim, and N.N. Mansour, Direct numerical simulation of turbulent channel flow up to  $Re_\tau = 590$ , *Phys. Fluids* **11**, 943 (1999); DNS data at <http://www.tam.uiuc.edu/Faculty/Moser/channel>.